Title: Electronic states and cation distributions of $MgAl_2O_4$ and $Mg_{0.4}Al_{2.4}O_4$ microwave dielectric ceramics

Authors: Susumu Takahashi, Hirotaka Ogawa, Akinori Kan

PII: S0955-2219(17)30561-7
DOI: http://dx.doi.org/10.1016/j.jeurceramsoc.2017.08.022
Reference: JECS 11417

To appear in: *Journal of the European Ceramic Society*

Received date: 16-2-2017
Revised date: 1-8-2017
Accepted date: 16-8-2017

Please cite this article as: Takahashi Susumu, Ogawa Hirotaka, Kan Akinori.Electronic states and cation distributions of MgAl2O4 and Mg0.4Al2.4O4 microwave dielectric ceramics.*Journal of The European Ceramic Society* http://dx.doi.org/10.1016/j.jeurceramsoc.2017.08.022

Electronic states and cation distributions of $MgAl_2O_4$ and $Mg_{0.4}Al_{2.4}O_4$ microwave dielectric ceramics

Susumu Takahashi, Hirotaka Ogawa, and Akinori Kan*

Graduate School of Science and Technology, Meijo University, Nagoya 468-8502, Japan

E-mail:akan@meijo-u.ac.jp

Abstract

The electronic state and microwave dielectric properties of $MgAl_2O_4$ prepared using solid-state (MA-S) and molten salt (MA-M) methods and those of $Mg_{0.4}Al_{2.4}O_4$ (M04A24) were investigated. The λ values, which correspond to the fraction of Al^{3+} cations in tetrahedral sites, for MA-S, MA-M, and M04A24 were 0.23, 0.41, and 0.60, respectively. In molecular orbital calculations, a larger overlap was observed between Al-3*s* or Al-3*p* in tetrahedral sites and O-2*p* orbitals for M04A24, and the bond order for Al–O at tetrahedral sites of M04A24 (0.241) was higher than those for MA-S (0.178) and MA-M (0.205). The dielectric constant, ε_r, for M04A24 (7.6) was lower than those

for MA-S and MA-M (both 7.9), and the highest quality factor, $Q \cdot f$, was obtained for M04A24 (235, 800 GHz). It was found that the covalency of the Al–O bonds in the MO_4 tetrahedra is closely related to the $Q \cdot f$ values of the present ceramics.

KEYWORDS: microwave dielectric properties; molecular orbital calculation; defect structure; cation distribution; $MgAl_2O_4$.

1. Introduction

Recently, microwave dielectric materials, which possess a low dielectric constant (ε_r), a high quality factor ($Q \cdot f$) and a near-zero temperature coefficient of resonant frequency (TCf) [1-6], have been characterized because they are considered suitable for application to wireless communication systems in the high-frequency region. The spinel-structured ceramic $MgAl_2O_4$ is one such material. Zheng *et al*. [7] reported ε_r and $Q \cdot f$ values for $MgAl_2O_4$ of 7.9 and 68,900 GHz, respectively. $MgAl_2O_4$ has an intermediate spinel structure with the general formula $(Mg_{1-\lambda}Al_{\lambda})[Mg_{\lambda}Al_{2-\lambda}]O_4$, where parentheses represent fourfold-coordinated sites and brackets represent sixfold-coordinated sites, and λ is referred to as the degree of inversion, ranging from 0 (normal spinel) to 1 (inverse spinel) [8-10]. The degree of inversion of $MgAl_2O_4$ has been investigated using ^{27}Al

nuclear magnetic resonance (NMR) and Raman spectroscopy [11-13]. In addition, Takahashi *et al*. [13] reported an enhancement in the $Q{\cdot}f$ of $MgAl_2O_4$ ceramics in which the Al^{3+} cation preferentially occupies the tetrahedral site. Moreover, Rietveld analysis of $MgAl_2O_4$ indicated that the preferential site occupation of Al^{3+} cations enhanced the covalency of the *M*–O bonds in the MO_4 tetrahedron (*M* = Mg and Al), leading to a decrease in the lattice parameters [13]. Thus, it has been suggested that the cation distribution in the $MgAl_2O_4$ lattice affects the covalency of cation–oxygen bonds and the microwave dielectric properties of the ceramics. Wittlinger *et al.* [14] and Ishii *et al*. [15] reported that the cation-vacancy-introduced $Mg_{0.4}Al_{2.4}V_{0.2}O_4$ (where *V* denotes the cation vacancy), like $MgAl_2O_4$, possesses a cubic spinel structure. It is expected that the introduction of cation vacancies in $MgAl_2O_4$ will facilitate the preferential occupation of the tetrahedral sites by Al^{3+} cations. However, the relationship between the electronic state and microwave dielectric properties of $MgAl_2O_4$ ceramics with cation vacancies remains unclear. Therefore, in this study, $Mg_{1-3x}Al_{2+2x}O_4$ ceramics (x = 0 and 0.2) were synthesized by a conventional solid-state reaction or the molten salt method, and the influence of cation distribution on the electronic state and microwave dielectric properties of these ceramics was investigated.

2. Experimental method

$MgAl_2O_4$ (MA) ceramics were prepared by a solid-state reaction (MA-S) and the molten salt method (MA-M), while the $Mg_{0.4}Al_{2.4}V_{0.2}O_4$ (M04A24) ceramic (V: cation vacancy) was prepared by the molten salt method. MgO (99.99%) and Al_2O_3 (99.9%) powders were weighed out in stoichiometric amounts and then ball-milled in a polyethylene bottle, using yittria-stabilized zirconia balls in ethanol for 24 h. The mixed slurries were dried and calcined at 1500°C for 4 h in air. In the case of MA-M and M04A24, the calcined powders were ground and mixed with LiCl (99.9%) in a weight ratio of 1:3, and the mixtures were transferred to an alumina crucible with an alumina lid and fired at 1200°C for 5 h. The fired mixtures were washed with distilled water and ethanol to remove residual salts and then dried at 80°C for 5 h in a drying oven. The powders were mixed with polyvinyl alcohol and uniaxially pressed into cylindrical pellets 12 mm in diameter and 7 mm in thickness at 100 MPa. Subsequently, these pellets were heated to 1600°C at a rate of 5°C/min and fired at 1600°C for 2-50 h in air. For convenience, $MgAl_2O_4$ ceramics prepared by the solid-state and molten salt methods will hereafter be referred to as MA-S-*n*h, MA-M-*n*h, and M04A24-*n*h, where *n* will denote the firing time. The crystalline phases of the fired samples were identified by X-ray powder diffraction (XRPD), using a Rigaku RINT-2000 diffractometer with

Cu Kα radiation at room temperature. The crystal structure of each crystalline phase was refined using the Rietveld analysis [16] software RETAN-FP [17] and the XRPD profiles for the Rietveld analysis were obtained by the step-scanning method in the 2θ range of 10°-120° with a step size of 0.03° and a counting time of 3.0 s/step. To investigate the cation distribution in the tetrahedral and octahedral sites, solid-state ^{27}Al magic angle spinning nuclear magnetic resonance (MAS-NMR) spectra were recorded on a JEOL ECA 500 spectrometer at room temperature with a spinning frequency of 12 kHz. X-ray absorption near-edge structure (XANES) spectra were obtained at the Mg *K*-edge by the total electron yield method at room temperature at beamline BL1N2 of the Aichi Synchrotron Radiation Center. The ε_r and $Q \cdot f$ values of the samples were measured by the Hakki and Coleman method [18, 19] at room temperature, using a vector network analyzer (Agilent 8720 ES). The *TCf* of each sample was determined from the resonant frequencies at 20 and 80°C. The apparent density of the sintered samples was estimated by the Archimedes method. The microstructure of the samples was investigated by field-emission scanning electron microscopy (FE-SEM; JEOL JSM-6330F). The electronic state of the ceramics was calculated by using the discrete variable Xα (DV-Xα) method [20], which is a first-principles calculation method, taking account of the Maldelung potential and symmetry orbital; the $(Mg_{11}Al_{22}O_{92})^{-106}$,

$(Mg_8Al_{25}O_{92})^{-93}$, and $(Mg_3Al_{28}O_{92})^{-94}$ cluster models in C_2 symmetry were employed for MA-S, MA-M, and M04A24, respectively.

3. Results and discussion

3.1. XRPD, XANES and NMR studies of $MgAl_2O_4$ and $Mg_{0.4}Al_{2.4}O_4$

Figure 1 shows XRPD profiles for MA-S-*n*h, MA-M-*n*h and M04A24-*n*h fired for 2 and 50 h. For both firing times, the XRPD profiles for all samples exhibited diffraction peaks corresponding to a cubic structure with the space group *Fd*3*m* (No. 227). The full width at half maximum (FWHM) values of the (311) planes of MA-S*n*h, MA-M*n*h and M04A24*n*h, tabulated in Table 1, provide a measure of the crystallinity of the ceramics. Lower FWHM values were obtained for samples fired at 1600°C for 50 h, and the FWHM value of M04A24-50h was lower than those of MA-M-50h and MA-S-50h. Moreover, the reflection peaks were found to shift in the case of MA and M04A24, suggesting that these peak shifts may be related to the variation in the distribution of Mg^{2+} and Al^{3+} cations in the tetrahedral and octahedral sites. To analyze the chemical composition of and confirm the presence of cation vacancies in M04A24, excitation fluorescence spectra were measured using synchrotron radiation and XANES spectra were measured for MA-S-50h and M04A24-50h (see Fig. 2). As seen from the

excitation fluorescence spectra in Fig. 2(a), the fraction of Mg was higher in MA-S-50h than in M04A24-50h, though the Al peak in the M04A24-50h spectrum was higher than that in the MA-S-50h spectrum. Si was detected owing to contamination. In the *K*-edge XANES spectra shown in Fig. 2(b), four peaks were observed at 1309, 1313, 1318, and 1331 eV for both ceramics, in good agreement with the peaks reported by Andrault *et al*. [21] and Li *et al*. [22], the latter of whom attributed the peak at 1313 eV (peak *b*) to the electronic transition from 1s to the empty bound 3*p* orbitals [23-25]. Moreover, the peaks at 1309, 1318, and 1331 eV, labelled as peaks *a*, *c*, and *e*, are due to the multiple scattering from the outermost coordination shells [22-25]. On the other hand, the spectra for M04A24-50h exhibited a peak at 1322 eV (peak *d*). This peak may be assigned to the cation vacancies in the $MgAl_2O_4$ lattice.

In order to determine the relationship between the cation distribution and firing time, the distributions of Al^{3+} in the tetrahedral and octahedral sites of MA-S-*n*h, MA-M-*n*h, and M04A24-*n*h were characterized by ^{27}Al NMR (see Fig. 3). The MA and M04A24 ceramics exhibited two signals, at approximately 10 and 70 ppm, which were assigned to octahedrally and tetrahedrally coordinated aluminum, respectively [26, 27]. The signal intensities at 70 ppm (10 ppm) were higher (lower) for the calcined ceramics than for the fired ceramics. Moreover, the signal intensities at 70 ppm (10 ppm) were slightly

lower (higher) for the ceramics fired for 2 h than for those fired for 50 h. These results suggest that the Al^{3+} cations in these ceramics preferentially occupy octahedral sites, depending on the firing time. To determine the proportions of Al^{3+} cations in tetrahedral and octahedral sites for MA-S-*n*h, MA-M-*n*h, and M04A24-*n*h, the λ values were estimated from the ^{27}Al NMR spectra and the equation

$$\frac{I(AlO_4)}{I(AlO_6)} = \frac{\lambda}{2 + 2x - \lambda}, \qquad (1)$$

where $I(AlO_4)$ and $I(AlO_6)$ denote the peak intensities of tetrahedrally and octahedrally coordinated aluminum, respectively [27]. Since x denotes the fraction of cation vacancies, $x = 0$ for MA-S-*n*h and MA-M-*n*h and $x = 0.2$ for M04A24-*n*h. The λ values for MA-S-*n*h, MA-M-*n*h, and M04A24-*n*h are summarized in Table 1. The λ values for the calcined ceramics were higher than those for the fired ceramics, and the λ values for the fired ceramics decreased with increasing firing time. The variation in λ value during firing suggests the redistribution of Al^{3+} and Mg^{2+} cations in the tetrahedral and octahedral sites, which leads to grain growth [13]. The λ value for M04A24-50h (λ = 0.60) was higher than those for MA-M-50h (λ = 0.41) and MA-S-50h (λ = 0.23). This indicated that the introduction of cation vacancies can promote the preferential occupation of tetrahedral sites by Al^{3+} cations.

3.2. Rietveld analysis and first-principles calculations

Based on the λ values, the site occupancies of MA-S-*n*h and MA-M-*n*h are estimated according to the general formula $(Mg_{1-\lambda}Al_{\lambda})[Mg_{\lambda}Al_{2-\lambda}]O_4$. Moreover, the site occupancy of M04A24-*n*h is also calculated, assuming that the cation vacancies are preferentially produced in the octahedral site [28,29]. The relationship between the cation distribution and cation vacancies of M04A24-*n*h are expressible by the general formula $(Mg_{0.8-\lambda}Al_{\lambda})[Mg_{\lambda-0.4}Al_{2.4-\lambda}V_{0.2}]O_4$. The crystal structure refinements of MA and M04A24 were performed using the Rietveld method, taking into account the estimated site occupancy. The lattice parameters of M04A24 are smaller than those of the MA ceramics, as listed in Table 2; the difference is presumably due to the difference in ionic radius between Mg^{2+} and Al^{3+} [30] and the difference in the proportion of Mg^{2+} and Al^{3+}. Moreover, the lattice parameters of MA and M04A24 decreased with increasing firing time. Since this decrease in the lattice parameters cannot be explained by the difference in the ionic radii of Mg^{2+} and Al^{3+}, the covalency (f_c/s) of the cation-oxygen bonds in the MO_4 (M = Mg and Al) tetrahedron and the MO_6 octahedron was calculated for MA-S-*n*h, MA-M-*n*h, M04A24-*n*h. The f_c of the cation-oxygen bonds was calculated using the refined atomic coordinates and the following equations:

$$s = (R/R_1)^{-N}, \qquad (2)$$

$$f_c = as^M, \qquad (3)$$

where s is the cation-oxygen bond strength and R represents the refined cation-oxygen bond length in MO_4 or MO_6. R_1 and N are empirical parameters that depend on the particular cation site and the cation-anion pair; R_1 = 1.622 and N = 4.29 [31]. The empirical constants a and M are 0.54 and 1.64, respectively [32]. The covalencies of the cation-oxygen bonds in MO_4 and MO_6 for MA-S-nh, MA-M-nh, and M04A24-nh are tabulated in Table 2. In all cases, while the covalencies of the M–O bonds in MO_6 were almost independent of firing time, those in MO_4 increased with firing time. The covalencies of the M–O bonds in MO_4 were higher (lower) for M04A24-nh (MA-S-nh) than for MA-M-nh. In the case of MO_6, the covalencies of the M–O bonds were almost the same (ca. 33.5%) for all samples. Thus, the decrease in the lattice parameters may be attributed to the increase in the covalency of the M–O bonds in MO_4, which arises from the preferential occupation of the tetrahedral sites by the Al^{3+} cations. In addition to Rietveld analysis, a first-principles calculation analysis was performed for MA-S-50h, MA-M-50h, and M04A24-50h to determine the electronic state of each ceramic, which is affected by the covalency of cation-oxygen bonds. As shown in Fig. 4, the cluster models $(Mg_{11}Al_{22}O_{92})^{-106}$, $(Mg_8Al_{25}O_{92})^{-93}$, and $(Mg_3Al_{28}O_{92})^{-94}$ with the estimated λ values were employed for MA-S-50h, MA-M-50h, and M04A24-50h, respectively. The total density of states (DOS) and energy-level diagrams of MA-S-50h, MA-M-50h, and

M04A24-50h are shown in Fig. 5. The energy-level diagrams reveal that the band gap of M04A24-50h (2.99 eV) is lower than those of MA-S-50h (3.81 eV) and MA-M-50h (3.79 eV). Tu *et al*. [28] investigated the effects of composition, *n*, on the electronic structure of the $MgO{\cdot}nAl_2O_3$ spinel model with cation vacancies, and they found that the band gap of the spinel decreased with increasing *n*. The band gap trend observed in the present study is consistent with their results. In the DOS of MA-S-50h, MA-M-50h, and M04A24-50h, the overlaps between the Al–3*s* or Al–3*p* and O–2*p* orbitals are observed for all the models, while the overlaps between the Al–3*s* or Al–3*p* and O–2*s* orbitals are very small. The overlap between the Mg–3*s* and O–2*s* or O–2*p* orbitals is negligibly small, which is indicative of the strong covalent bonding between aluminum and oxygen. In the tetrahedral site, the overlap between the Al–3*s* or Al–3*p* and O–2*p* orbitals seems to be larger for M04A24-50h than for MA-M-50h and MA-S-50h. Moreover, the bond order of Al–O at tetrahedral site, which is related to strength of the covalent bonds, is higher for M04A24-50h (0.241) than for MA-S-50h (0.178) and MA-M-50h (0.205). This is presumably because of the preferential occupation by Al^{3+} of the tetrahedral site through the introduction of cation vacancies. Thus, the variations in the covalency of *M*–O bonds in the MO_4 tetrahedron, as revealed by Rietveld analysis, are associated with the strong covalent bonding between the Al–3*s* or Al–3*p* orbitals in

the tetrahedral site and O–2*p* orbitals.

3.3. Microwave dielectric properties of $MgAl_2O_4$ and $Mg_{0.4}Al_{2.4}O_4$

Figure 6 (a) shows the relative densities of MA-S-*n*h, MA-M-*n*h, and M04A24-*n*h. Upon increasing the firing time from 2 to 5 h, the relative density of MA-S-*n*h increased from 92 to 96%, while those of MA-M-*n*h and M04A24-*n*h increased from approximately 94 to 96%. The relative densities of all samples leveled off above a firing time of 5 h. The morphological changes in MA-S-*n*h, MA-M-*n*h, and M04A24-*n*h were also observed in the FE-SEM images shown in Fig. 7. The grain sizes of MA and M04A24 strongly depended on the firing time; with increasing firing time, the grain size of MA-S-*n*h increased from 10 to 20 μm, while the grain sizes of MA-M*n*h and M04A24*n*h increased from 25 to 50 μm. This grain growth was presumably related to the redistribution of Mg^{2+} and Al^{3+} during firing. The effects of firing time on the ε_r and $Q{\cdot}f$ of MA and M04A24 are shown in Fig. 6. The variations in ε_r paralleled those in relative density; with increasing firing time, the ε_r of MA-S-*n*h increased from 7.4 to 7.9, while those of MA-M-*n*h and M04A24-*n*h increased slightly from 7.8 to 7.9 and from 7.4 to 7.6, respectively. The lower ε_r value of M04A24 may be related to the introduction of cation vacancies and to the increase in the fraction of aluminum, which has a lower ionic polarizability (0.73 $Å^3$) than Mg^{2+} (1.33 $Å^3$) [33]. As the firing time

increased, the $Q{\cdot}f$ values of all samples increased markedly between 2 and 5 h of firing, increasing only gradually in the 5-50 h range. Takahashi *et al*. [13] reported that the high crystallinity of $MgAl_2O_4$ enhances its $Q{\cdot}f$ value. Therefore, the marked increase in the $Q{\cdot}f$ values of MA and M04A24 may be due to the higher crystallinities of these ceramics (see Table 1). On the other hand, the $Q{\cdot}f$ of M04A24-50h (235,800 GHz) was higher than those of MA-S-50h and MA-M-50h. This is thought to be due to the preferential occupation of tetrahedral sites by Al^{3+} cations in the case of M04A24-50h, which leads to an increase in the covalency of the *M*-O bond in the MO_4 tetrahedron, since the cation distribution in the spinel lattice affects the $Q{\cdot}f$ values of ceramics [13,34,35]. The *TCf* values of MA-S-*n*h, MA-M-*n*h, and M04A24-*n*h were also measured. No significant differences were observed; the *TCf* values were approximately –60 ppm/°C in all three cases. Thus, the effect of cation distribution on *TCf* value is considered to be small.

4. Conclusion

The microwave dielectric properties and crystal structures of MA-S, MA-M and M04A24 ceramics were investigated. The ^{27}Al NMR data revealed a higher λ value for M04A24 (0.60) than for MA-S (0.23) and MA-M (0.41); the Al^{3+} cation in the M04A24

lattice preferentially occupied the tetrahedral site owing to the introduction of cation vacancies. Rietveld refinement and first-principles calculation analyses suggested that the overlap between Al in the tetrahedral site and the O–2*p* orbitals was larger for M04A24-50h than for MA-M-50h and MA-S-50h; the preferential occupation of the tetrahedral site by Al^{3+} enhanced the covalency of Al–O bonds in the MO_4 tetrahedron (*M* = Mg and Al), leading to decreases in lattice parameter. The ε_r of M04A24 (7.6) was lower than those of MA-S and MA-M (both 7.9). Although the $Q \cdot f$ of MA and M04A24 increased with firing time, the highest $Q \cdot f$ value was obtained for M04A24-50h ($Q \cdot f$ = 235,800 GHz). Thus, it is concluded that the preferential occupation of tetrahedral sites by Al^{3+} through the introduction of cation vacancies and molten salt synthesis enhances the $Q \cdot f$ of spinel-structured ceramics.

Acknowledgment

This work was supported by a Grant-in-Aid from the Japan Society for the Promotion of Science (JSPS, Research Fellow Grant Number JP16J11394).

References

[1] M. Ando, H. Ohsato, I. Kagomiya, and T. Tsunooka, "Quality Factor of Forsterite for Ultrahigh Frequency Dielectrics Depending on Synthesis Process," J*pn. J. Appl. Phys*. **47** [9] 7729-7731 (2008).

[2] I. Kagomiya, Y. Matsuda, K. Kakimoto and H. Ohsato, "Microwave Dielectric Properties of YAG Ceramics", *Ferroelectrics.* 387 1-6 (2009).

[3] Y. Guo, H. Ohsato, and K. Kakimoto, "Characterization and Dielectric Behavior of Willemite and TiO_2-Doped Willemite Ceramics at Millimeter-Wave Frequency," *J. Eur. Ceram. Soc.*, **26** [10] 1827-1830 (2006).

[4] K. P. Surendran, P. V. Bijumon, P. Mohanan, and M. T. Sebastian, "(1-*x*)$MgAl_2O_4$-xTiO_2 dielectrics for microwave and millimeter wave applications", *Appl. Phys*. *A.* **00** 1-4 (2005).

[5] S. Wu, C. Jiang, Y. Mei, and W. Tu, "Synthesis and Microwave Dielectric Properties of Sm_2SiO_5 Ceramics," *J. Am. Ceram. Soc*., **95** [1] 37-40 (2012).

[6] H. Ogawa, A. Kan, S. Ishihara, and Y. Higashida, "Crystal Structure of Corundum Type $Mg_4(Nb_{2-x}Ta_x)O_9$ Microwave Dielectric Ceramics with Low Dielectric Loss," *J. Eur. Ceram. Soc*. **23** [14] 2485-2488 (2003).

[7] C. W. Zheng, S. Y. Wu, X. M. Chen, and K. X. Song, "Modification of $MgAl_2O_4$

Microwave Dielectric Ceramics by Zn Substitution," *J. Am. Ceram. Soc*., **90** [5] 1483-1486 (2007).

[8] H. Cynn, S. K. Sharma, T. F. Cooney, and M. Nicol, "High-temperature Raman Investigation of Order-disorder Behavior in the $MgAl_2O_4$ Spinel", *Physical Review B*. **45** 500-502 (1992).

[9] M. P. O'horo, A. L. Frisillo, and W. B. White, "Lattice vibrations of $MgAl_2O_4$ Spinel", *J. Phys. Chem. Solids*. **34** 23-28 (1973).

[10] S. P. Slotznick and S. –H. Shim, "In situ Raman Spectroscopy Measurements of $MgAl_2O_4$ Spinel up to 1400 °C", *Am. Mineral*. **93** 470-476 (2008).

[11] R. L. Millard, R. C. Peterson, and B. K. Hunter, "Temperature Dependence of Cation Disorder in $MgAl_2O_4$ Spinel Using ^{27}Al and ^{17}O Magic-Angle Spinning NMR," *Amer. Mineral*, **77** 44-52 (1992).

[12] A. Chopelas, and A. M. Hofmeister, "Vibrational Spectroscopy of Aluminate Spinels at 1 atm and of $MgAl_2O_4$ to Over 200 kbar," *Phys. Chem. Minerals*, **18** 279-293 (1991).

[13] S. Takahashi, A. Kan, and H. Ogawa, "Microwave Dielectric Properties and Crystal Structure of Spinel-Structured $MgAl_2O_4$ Ceramics Synthesized by A Molten-Salt Method," *J. Eur. Ceram. Soc.*, **37** 1001-1006 (2017).

[14] J. Wittlinger, S. Werner, and H. Schulz, "Pressure-Induced Order-Disorder Phase Transition of Spinel Single Crystals," Acta Cryst. B, **54** 714-721 (1998).

[15] M. Ishii, J. Hiraishi, and T. Yamanaka, "Structure and Lattice Vibrations of Mg-Al Spinel Solid Solution," *Phys. Chem. Minerals*, **8** [2] 64 (1982).

[16] H. M. Rietveld, "A Profile Refinement Method for Nuclear and Magnetic Structures," *J. Appl. Crystallor*., **2** 65-71 (1969).

[17] F. Izumi, and K. Momma, "Three-Dimensional Visualization in Powder Diffraction," Solid State Phenom., **130** 15 (2007).

[18] B. W. Hakki, and P. D. Coleman, "A Dielectric Resonator Method of Measuring Inductive Capacities in the Millimeter Range," *I. R. E. Trans, Microwave Theory Tech*. **8** [4] 402-410 (1960).

[19] Y. Kobayashi, and M. Katoh, "Microwave Measurement of Dielectric Properties of Low-Loss Materials by the Dielectric Rod Resonator Method," *IEEE Trans. Microwave Theory Tech*., **33** [7] 586 (1985).

[20] H. Adachi, M. Tsukada, and C. Satoko, "Discrete Variational Xα Cluster Calculations. I. Application to Metal Cluster", *J. Phys. Soc. Jpn*. **45** 875-883 (1978).

[21] D. Andrault, D. R. Neuville, A. –M. Flank, and Y. Wang, "Cation Sites in Al-rich

$MgSiO_3$ Perovskites", *Am. Mineral*. **83** 1045-1053 (1998).

[22] D. Li, M. S. Peng, T. Murata, "Coordination and Local Structure of Magnesium in Silicate Minerals and Glasses: MgK-edge XANES study", *Can. Mineral.* **37** 199-206 (1999).

[23] D. R. Neuville, D. Ligny, L. Cormier, G. S. Henderson, J. Roux, A. –M. Flank, and P. Lagarde, "The Crystal and Melt Structure of Spinel and Alumina at High Temperature: An in-situ XANES study at the Al and Mg K-edge", *Geochimica Cosmochimica Acta*. **73** 3410-3422 (2009).

[24] T. Tanaka, and H. Yoshida, "Study of Dehydration of Magnesium Hydroxide", *J. Phys. Chem*. **99** 10890-10896 (1995).

[25] S. M. Davis, Y. Zhou, M. Freeman, D. A. Fischer, G. M. Meitzner, J. L. Grand, "Carbon K-Edge X-Ray Absorption Spectroscopy of Gas Oil Derived Coke Deposits in LZ-210 Zeolite", *J. Catal*. **139** 322-325 (1993).

[26] E. S. Blaakmeer, F. Rosciano, and E. R. H. Eck, "Lithium Doping of $MgAl_2O_4$ and $ZnAl_2O_4$ Investigated by High-Resolution Solid State NMR," *J. Phys. Chem. C*, **119** [14] 7565-7577 (2015).

[27] V. Šepelák, S. Indris, I. Bergmann, A. Feldhoff, K. D. Becker, and P. Heitjans, "Nonequilibrium Cation Distribution in Nanocrystalline $MgAl_2O_4$ Spinel Studied

by ^{27}Al Magic-Angle Spinning NMR," *Solid. State. Ionics*, **177** [26-32] 2487-2490 (2006).

[28] B. Tu, H. Wang, X. Liu, W. Wang, Z. Fu, "Theoretical Predictions of Composition-Dependent Structure and Properties of Alumina-Rich Spinel", *J. Eur. Ceram. Soc.*, **36** 1073-1079 (2016).

[29] R. Basso, S. Carbonin and A. D. Giusta, "Cation and vacancy distribution in a synthetic defect spinel", *Z. Kristallogr.*, **194** 111-119 (1991).

[30] R. D. Shannon, "Revised Effective Ionic Radii and Systematic Studies of Interatomic Distances in Halides and Chalcogenides," *Acta Crystallogr*. *A*, **32** [5] 751-767 (1976).

[31] I. D. Brown and K. K. Wu, "Empirical Parameters for Calculating Cation-Oxygen Bond Valences," *Acta Crystallogr. Sect. B*, **32** [7] 1957-1959 (1976).

[32] I. D. Brown, and R. D. Shannon, "Empirical Bond-Strength-Bond-Length Curves for Oxides," *Acta Crystallogr. Sect. A*, **29** [3] 266-282 (1973).

[33] R. D. Shannon, "Dielectric Polarizabilities of Ions in Oxides and Fluorides," *J. Appl. Phys*., **73** [1] 348-366 (1993).

[34] E. Koga, and H. Moriwake, "Effects of Superlattice Ordering and Ceramic Microstructure on the Microwave *Q* Factor of Complex Perovskite-Type Oxide

$Ba(Zn_{1/3}Ta_{2/3})O_3$," *J. Ceram. Soc. Jpn*., **111** [10] 767-775 (2003).

[35] E. Koga, H. Moriwake, K. Kakimoto, and H. Ohsato, "Influence of Composition Deviation from Stoichiometric $Ba(Zn_{1/3}Ta_{2/3})O_3$ on Superlattice Ordering and Microwave Quality Factor *Q*," *J. Ceram. Soc. Jpn*., **113** [2] 172-178 (2005).

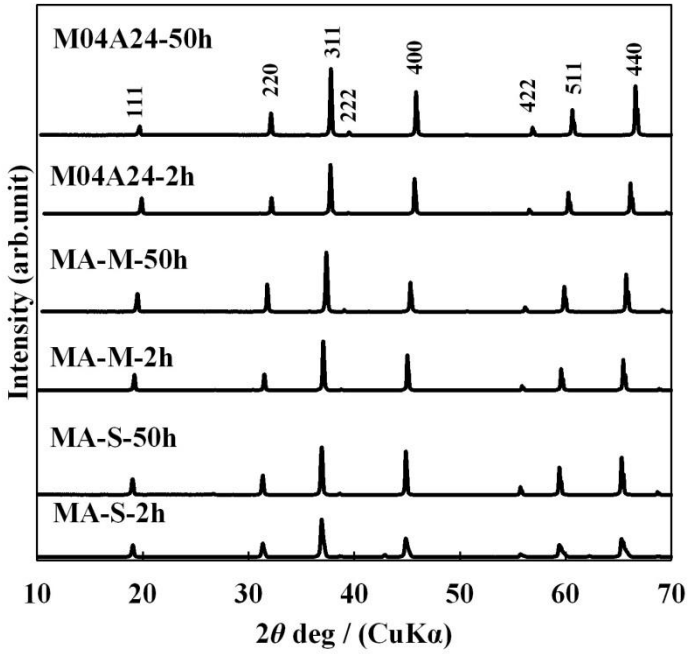

Fig.1. XRPD profiles of MA-S-*n*h, MA-M-*n*h and M04A24-*n*h fired at 1600 °C for 2 and 50 h.

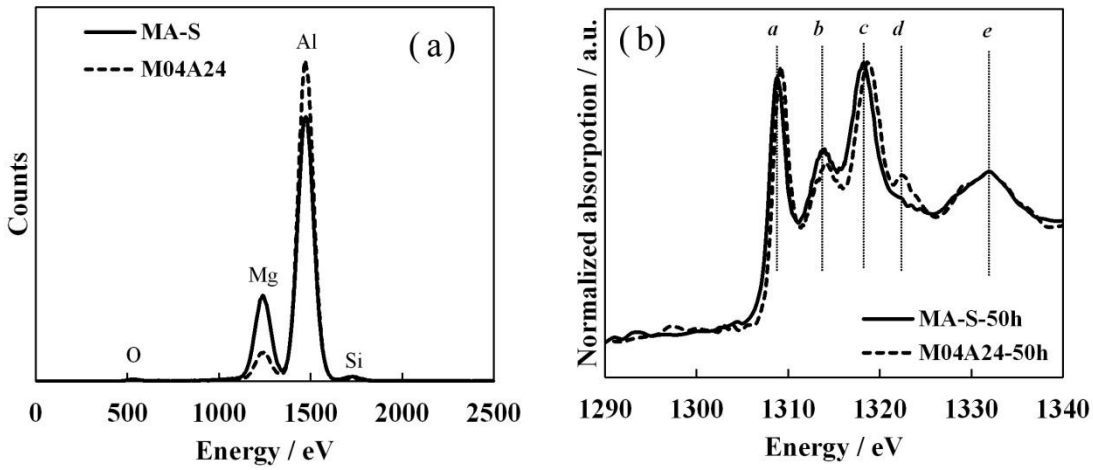

Fig. 2. (a) Excitation fluorescence and (b) Mg *K*-edge XANES spectra of MA-S-50h and M04A24-50h.

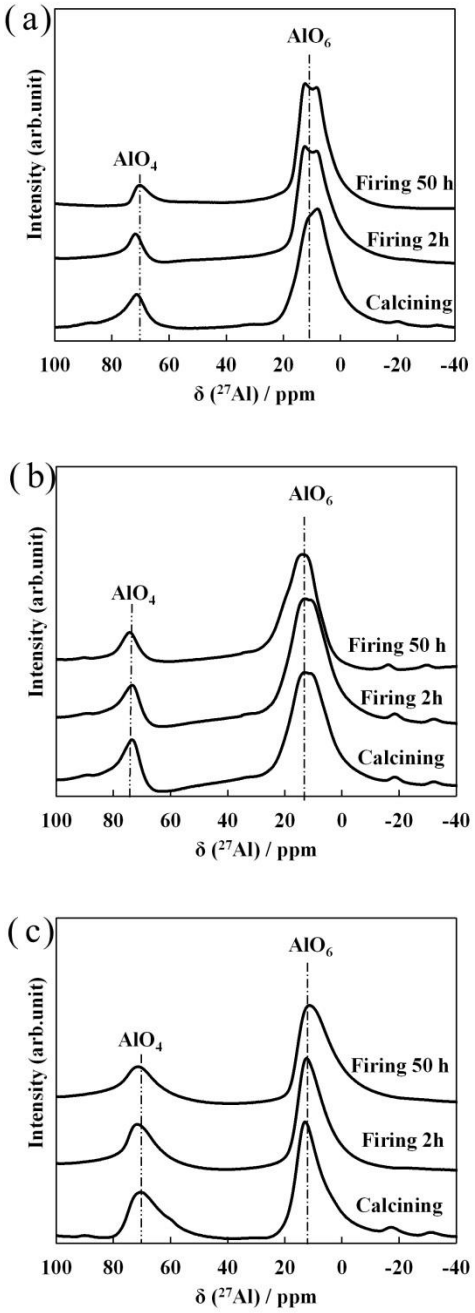

Fig. 3. ^{27}Al NMR spectra of (a) MA-S, (b) MA-M and (c) M04A24 fired at 1600 °C for 2 and 50 h.

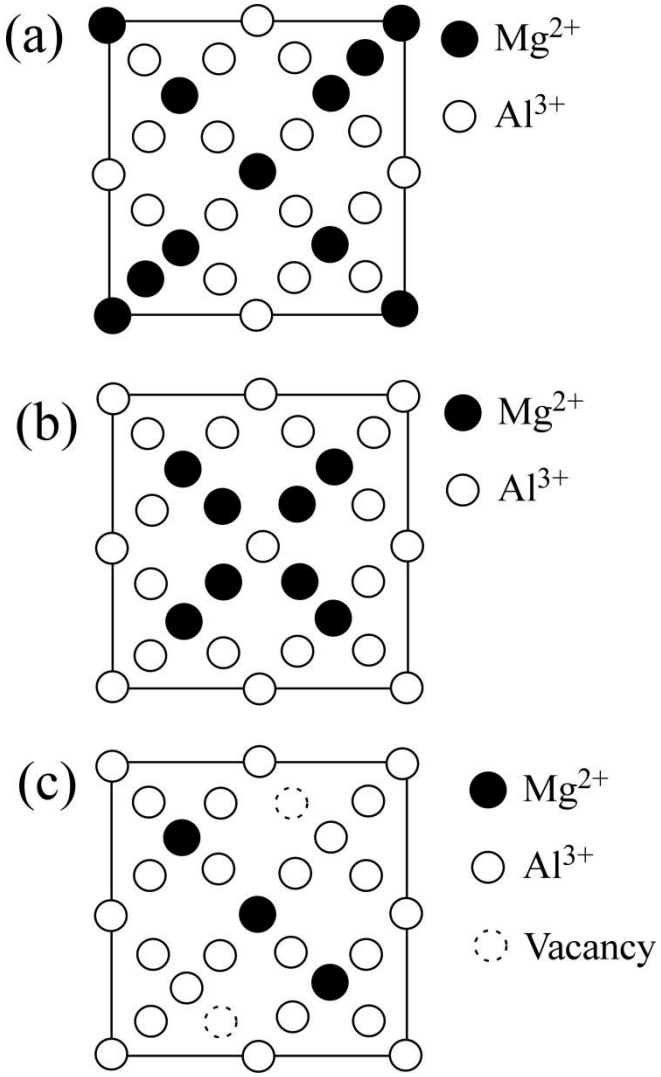

Fig. 4. Schematic diagrams of (a) $(Mg_{11}Al_{22}O_{92})^{-106}$, (b) $(Mg_8Al_{25}O_{92})^{-93}$, and (c) $(Mg_3Al_{28}O_{92})^{-94}$ cluster models, viewed along the [100] direction.

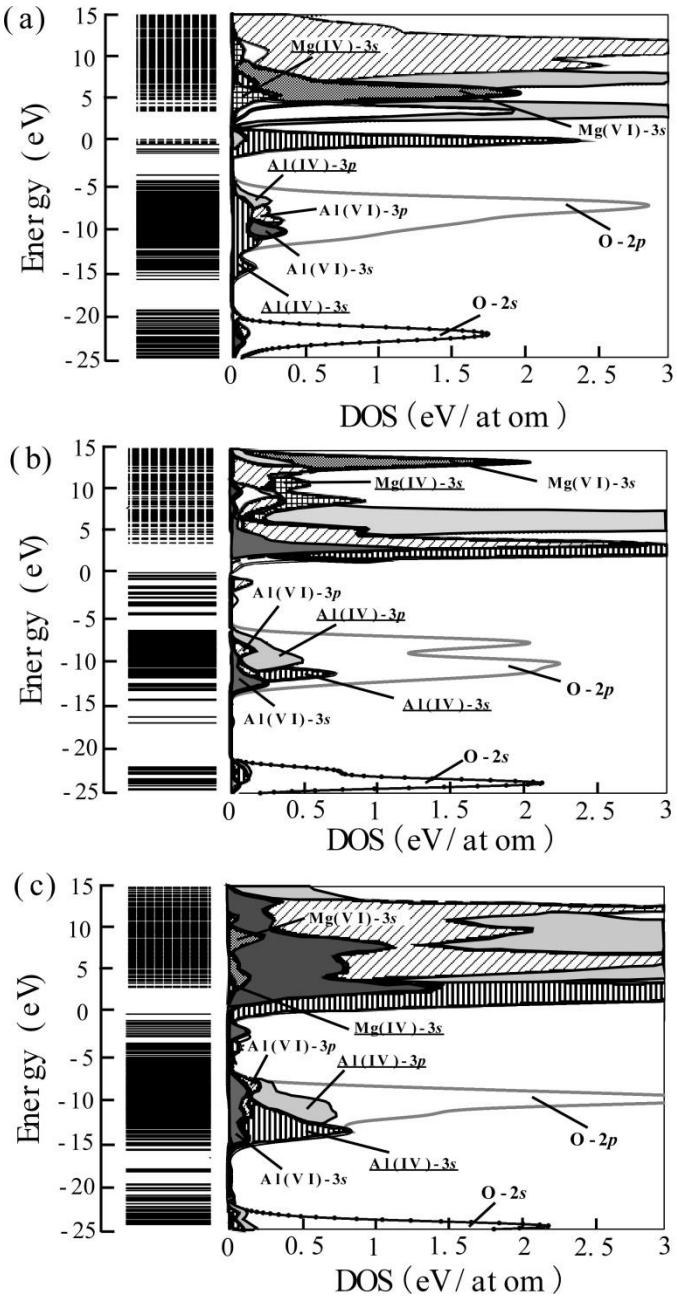

Fig. 5. Energy level diagrams and partial density of states of (a) MA-S, (b) MA-M and (c) M04A24 fired at 1600 °C for 50 h.

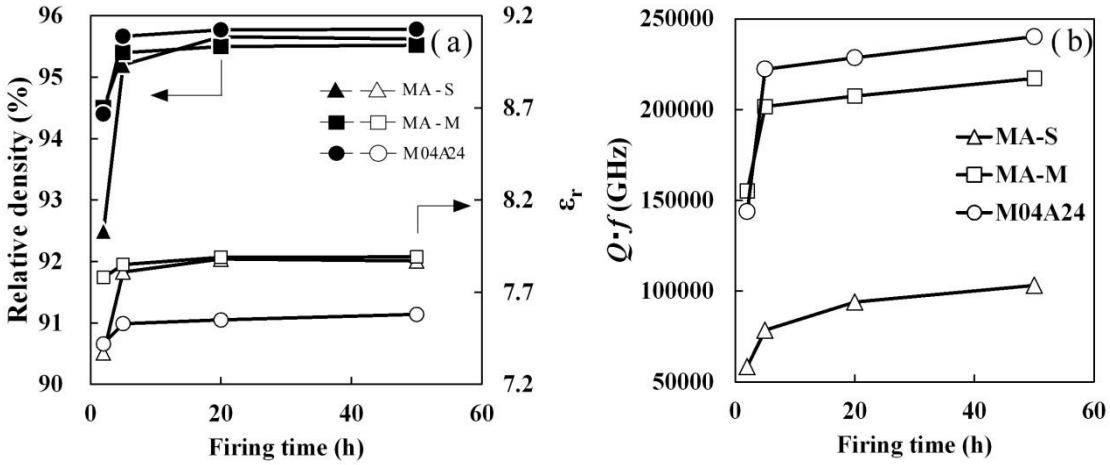

Fig. 6. Effects of firing time on (a) relative densities and ε_r and (b) $Q \cdot f$ of MA-S, MA-M and M04A24.

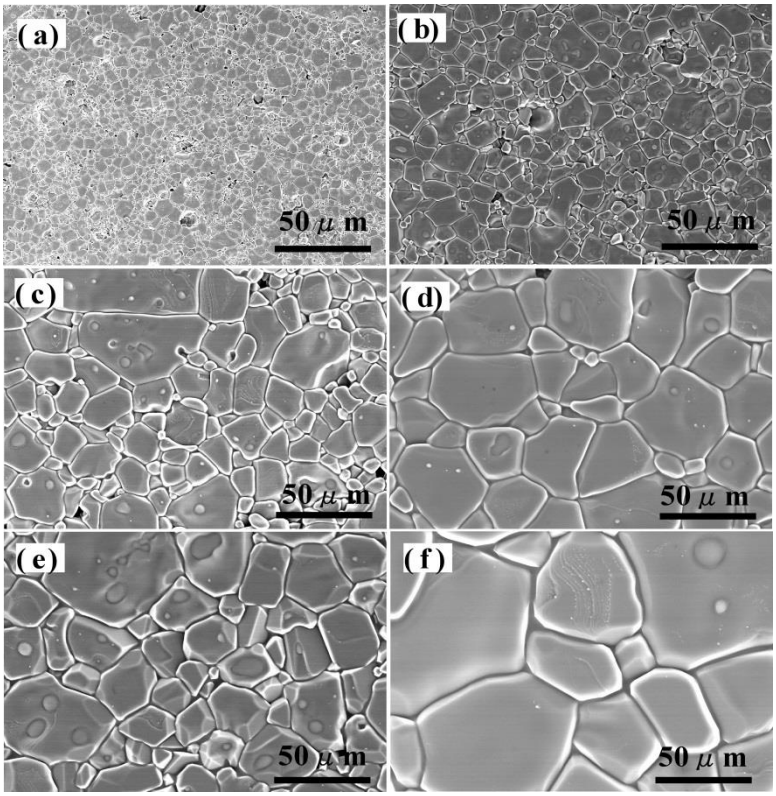

Fig. 7. FE-SEM images of (a) MA-S-2h, (b) MA-S-50h, (c) MA-M-2h, (d) MA-M-50h, (e) M04A24-2h and (f) M04A24-50h .

Table 1 Fraction of Al^{3+} cation in tetrahedral sites (λ) and FWHM values in (311) plane of MA-S-*n*h, MA-M-*n*h and M04A24-*n*h.

Sample	Process	Firing time (h)	FWHM (°)	Site occupancy of Al^{3+} cation in tetrahedral site λ
MA-S	Calcining	5	0.285	0.33
	Firing	2	0.168	0.26
		5	0.156	0.25
		50	0.154	0.23
MA-M	Calcining	5	0.213	0.59
	Firing	2	0.140	0.45
		5	0.139	0.42
		50	0.136	0.41
M04A24	Calcining	5	0.215	0.75
	Firing	2	0.142	0.65
		5	0.135	0.60
		50	0.132	0.60

Table 2 Lattice parameter, volume and covalency of *M*-O bonds in MO_4 tetrahedra and MO_6 octahedra (*M* = Mg and Al) of MA-S-*n*h, MA-M-*n*h and M04A24-*n*h.

Sample	Firing time (h)	Lattice parameter *a* (Å)	Covalency of *M*-O bonds in MO_4 tetrahedra (%)	Covalency of *M*-O bonds in MO_6 octahedra (%)
MA-S	2	8.0800(2)	33.4	33.5
	5	8.0745(4)	33.8	33.4
	50	8.0711(2)	34.0	33.5
MA-M	2	8.0723(3)	34.3	33.7
	5	8.0634(6)	35.3	33.3
	50	8.0534(6)	35.5	33.4
M04A24	2	7.9866(5)	37.8	33.5
	5	7.9644(2)	39.0	33.3
	50	7.9632(1)	39.3	33.2